Optical circuits from anisotropic films

Huikan Liu, Shivanand, and Kevin J. Webb*
School of Electrical and Computer Engineering, Purdue University, 465 Northwestern Avenue, West Lafayette, Indiana 47907-2035, USA
(Received 13 November 2008; published 31 March 2009)

The theory for inductive and capacitive elements realized from anisotropic slabs is developed. These elements are shown to have low sensitivity to angle of incidence and nondispersive performance. It is therefore possible to realize optical circuits that perform more effectively than would be possible with isotropic materials. Low-pass filtering and antireflection examples are given. Desirable anisotropy can be achieved using a metal-insulator stack operating in the effective-medium metamaterial regime. The approach allows circuit synthesis at optical wavelengths.

DOI: 10.1103/PhysRevB.79.094203 PACS number(s): 42.25.Bs, 42.79.−e, 78.67.−n

I. INTRODUCTION

The range of available electromagnetic material properties has been dramatically broadened by the advent of metamaterials.[1–3] Artificially engineered media provide important parameter values that allow applications not possible with naturally occurring materials, for instance, negative refraction, imaging with subwavelength resolution, and cloaking.[1,4–7] While a negative index slab can provide growth in the evanescent fields and hence better resolution, achieving such a material at optical frequencies with suitable low-loss properties is challenging. An anisotropic slab has been proposed for subwavelength imaging.[8–11] Such anisotropy can be achieved with a metal-insulator stack or wire media,[8–10,12,13] making it practical for implementation at optical frequencies.

Here, we identify the features of equivalent circuit elements that can be achieved with anisotropic slabs. The parameters for these slabs can be obtained at optical frequencies using a metal-insulator stack. Unlike isotropic materials, the circuit elements from anisotropic slabs are independent of wavelength (if material dispersion can be neglected) and incident angle, with appropriate anisotropy. In other recent work, the realization of circuit nanoelements in the optical domain using nanoparticles has been proposed.[14,15] Motivation for that work, as in ours, was that new devices become possible based on the understanding provided by the equivalent circuit elements. We show filter and antireflection coatings that operate based on the principles we describe.

II. LUMPED OPTICAL CIRCUIT ELEMENTS

We consider the scattering properties of a single slab with a uniaxial dielectric tensor having $\epsilon_k=\epsilon_k'+i\epsilon_k''$ $(k=x,y,z)$, as in Fig. 1. Such a dielectric tensor can be achieved from the effective dielectric parameters of a metal-insulator stack, under the quasistatic approximation, where the wavelength is large relative to the period and that there are a sufficient number of periods.[8–10,13]

The transverse-magnetic (TM) incident wave (the extraordinary wave, having H_y, referring to Fig. 1) has a dispersion relation given by $k_x^2\epsilon_z^{-1}+k_z^2\epsilon_x^{-1}=k_0^2$. On the other hand, the

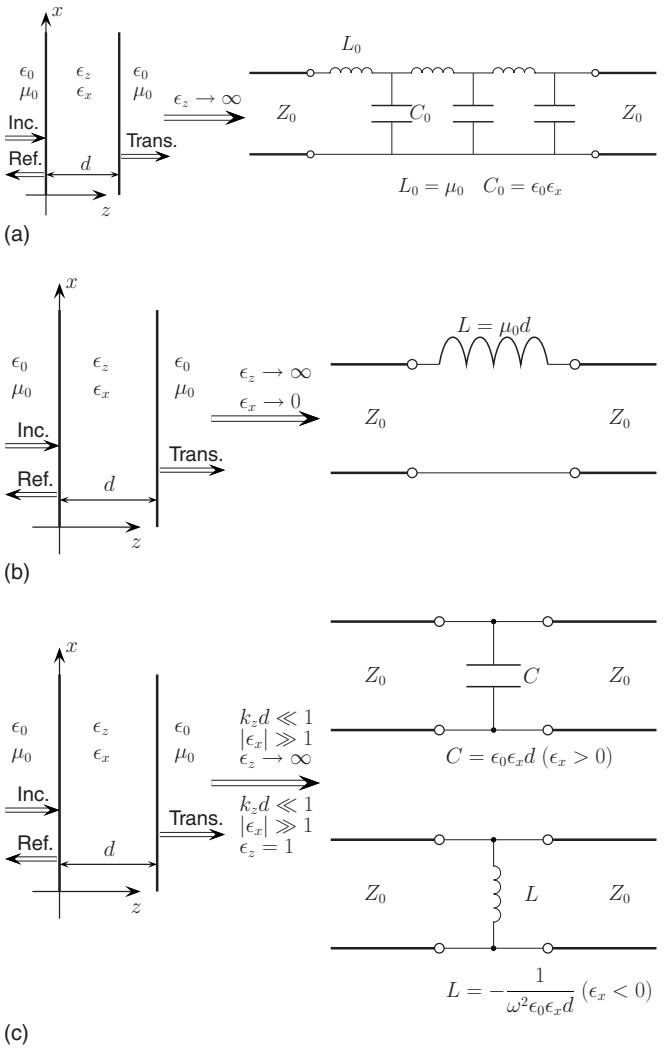

FIG. 1. (a) Equivalent transmission line in the optical regime from envisioning an anisotropic slab when $\epsilon_z\to\infty$. (b) An anisotropic slab with $\epsilon_z\to\infty$, $\epsilon_x\to 0$ could play the role of an optical lumped inductor in response to incident TM waves. (c) Equivalent shunt capacitor (inductor) when $k_z d\ll 1$, $\epsilon_x\gg 1(|\epsilon_x|\gg 1, \epsilon_x<0)$, $\epsilon_z\to\infty$ (or $\epsilon_z=1$).

transverse-electric (TE) wave (the ordinary wave, with E_y) is governed by the dispersion relation $k_x^2+k_{z0}^2=\epsilon_y k_0^2$. We assume free space regions surrounding the slab, but our results can be generalized for the slab being embedded in background material(s). For a slab of thickness d, the plane-wave transmission coefficient $[T(k_x)]$ and reflection coefficient $[\Gamma(k_x)]$ for H_y are

$$T(k_x)=\frac{1}{\cos(k_z d)-\frac{i}{2}\left(\frac{Z_s}{Z_0}+\frac{Z_0}{Z_s}\right)\sin(k_z d)}, \tag{1}$$

$$\Gamma(k_x)=\frac{\frac{i}{2}\left(\frac{Z_s}{Z_0}-\frac{Z_0}{Z_s}\right)\sin(k_z d)}{\cos(k_z d)-\frac{i}{2}\left(\frac{Z_s}{Z_0}+\frac{Z_0}{Z_s}\right)\sin(k_z d)}, \tag{2}$$

where $Z_s=k_z/(\omega\epsilon_x\epsilon_0)$ and $Z_0=k_{z0}/(\omega\epsilon_0)$ denote the characteristic impedances of the slab and the surrounding medium, respectively, with ϵ_0 as the free space permittivity, and we use time convention $\exp(-i\omega t)$. After incorporating the dispersion relations into Eqs. (1) and (2),

$$T(k_x)=\frac{1}{\cos\left[\sqrt{\epsilon_x\left(k_0^2-\frac{k_x^2}{\epsilon_z}\right)}d\right]-\frac{i}{2}\left[\sqrt{\frac{\epsilon_x(k_0^2-k_x^2)}{k_0^2-\frac{k_x^2}{\epsilon_z}}}+\sqrt{\frac{k_0^2-\frac{k_x^2}{\epsilon_z}}{\epsilon_x(k_0^2-k_x^2)}}\right]\sin\left[\sqrt{\epsilon_x\left(k_0^2-\frac{k_x^2}{\epsilon_z}\right)}d\right]}, \tag{3}$$

$$\Gamma(k_x)=\frac{\frac{i}{2}\left(\sqrt{\frac{k_0^2-\frac{k_x^2}{\epsilon_z}}{\epsilon_x(k_0^2-k_x^2)}}-\sqrt{\frac{\epsilon_x(k_0^2-k_x^2)}{k_0^2-\frac{k_x^2}{\epsilon_z}}}\right)\sin\left[\sqrt{\epsilon_x\left(k_0^2-\frac{k_x^2}{\epsilon_z}\right)}d\right]}{\cos\left[\sqrt{\epsilon_x\left(k_0^2-\frac{k_x^2}{\epsilon_z}\right)}d\right]-\frac{i}{2}\left[\sqrt{\frac{\epsilon_x(k_0^2-k_x^2)}{k_0^2-\frac{k_x^2}{\epsilon_z}}}+\sqrt{\frac{k_0^2-\frac{k_x^2}{\epsilon_z}}{\epsilon_x(k_0^2-k_x^2)}}\right]\sin\left[\sqrt{\epsilon_x\left(k_0^2-\frac{k_x^2}{\epsilon_z}\right)}d\right]}. \tag{4}$$

For $k_0^2 \gg k_x^2/\epsilon_z$, $k_z^2=\epsilon_x(k_0^2-k_x^2/\epsilon_z)\approx\epsilon_x k_0^2$, and k_z is real for all k_x, ignoring loss. In this case, Eqs. (3) and (4) become

$$T(k_x)=\left[\cos(\sqrt{\epsilon_x}k_0 d)-\frac{i}{2}\left(\sqrt{\frac{\epsilon_x(k_0^2-k_x^2)}{k_0^2}}+\sqrt{\frac{k_0^2}{\epsilon_x(k_0^2-k_x^2)}}\right)\sin(\sqrt{\epsilon_x}k_0 d)\right]^{-1}, \tag{5}$$

$$\Gamma(k_x)=\frac{\frac{i}{2}\left(\sqrt{\frac{k_0^2}{\epsilon_x(k_0^2-k_x^2)}}-\sqrt{\frac{\epsilon_x(k_0^2-k_x^2)}{k_0^2}}\right)\sin(\sqrt{\epsilon_x}k_0 d)}{\cos(\sqrt{\epsilon_x}k_0 d)-\frac{i}{2}\left(\sqrt{\frac{\epsilon_x(k_0^2-k_x^2)}{k_0^2}}+\sqrt{\frac{k_0^2}{\epsilon_x(k_0^2-k_x^2)}}\right)\sin(\sqrt{\epsilon_x}k_0 d)}. \tag{6}$$

A perfect lens [$T=1$ in Eq. (5)] can be achieved with a thickness given by the resonance condition

$$\sqrt{\epsilon_x}k_0 d=n\pi, \quad n=1,2,\ldots. \tag{7}$$

More specifically, $k_z d=2n\pi$ results in a zero-phase-shift perfect lens, whereas $k_z d=(2n+1)\pi$ leads to a π-phase-shift perfect lens. Regardless of k_x, $E_z=0$ in the slab [$E_z/H_y=k_x/(\omega\epsilon_0\epsilon_z)=0$], and the field has only transverse-electric and transverse-magnetic field components [and is thus a transverse electromagnetic (TEM) mode], as exists in ideal transmission lines and as found for wire media and metallodielectric layered structures.[12,16] Writing $Z_s=\sqrt{L_0/C_0}=k_z/(\omega\epsilon_x\epsilon_0)$ and $k_z=\omega\sqrt{L_0C_0}=k_0\sqrt{\epsilon_x}$ leads to $L_0=\mu_0$ and $C_0=\epsilon_0\epsilon_x$, and hence the distributed equivalent circuit model of

Fig. 1(a). Equation (7) is a half-wavelength line condition, under which the magnitudes of electric and magnetic fields remain preserved across the slab, yielding a perfect slab lens. Using $Z_s=\eta_0/\sqrt{\epsilon_x}$, with η_0 as the free space wave impedance, quarter-wave antireflection coatings can be designed which are independent of k_x, i.e., independent of the angle of incidence. By adjustment of d and real ϵ_x, it is possible to produce an antireflection coating for a material having complex ϵ, again independent of k_x.

Enforcing $\epsilon_x \to 0$ in Eqs. (3) and (4),

$$T(k_x)=\frac{1}{1-\frac{i}{2}\frac{\left(k_0^2-\frac{k_x^2}{\epsilon_z}\right)d}{\sqrt{k_0^2-k_x^2}}}, \quad \Gamma(k_x)=\frac{\frac{i}{2}\frac{\left(k_0^2-\frac{k_x^2}{\epsilon_z}\right)d}{\sqrt{k_0^2-k_x^2}}}{1-\frac{i}{2}\frac{\left(k_0^2-\frac{k_x^2}{\epsilon_z}\right)d}{\sqrt{k_0^2-k_x^2}}}. \tag{8}$$

A series impedance Z in a transmission line having characteristic impedance Z_0 has current transmission (T_I) and reflection (Γ_I) coefficients given by[17]

$$T_I=\frac{1}{1+\frac{Z}{2Z_0}}, \quad \Gamma_I=\frac{-\frac{Z}{2Z_0}}{1+\frac{Z}{2Z_0}}. \tag{9}$$

Comparing Eqs. (8) and (9) indicates that, in the limit $\epsilon_x \to 0$, the anisotropic slab behaves like a lumped series inductor with the k_x-dependent inductance

$$L=\mu_0 d\left[1-\frac{1}{\epsilon_z}\left(\frac{k_x}{k_0}\right)^2\right]. \tag{10}$$

Applying $\epsilon_z \to \infty$ in Eq. (10) leads to the simple series k_x-independent inductor $L=\mu_0 d$ [see Fig. 1(b)]. This equivalence is approximately true for $k_0\sqrt{\epsilon_x}d \ll 1$ and large ϵ_z.

With $\epsilon_z \to \infty$ and $\epsilon_x \gg 1$ in Eqs. (3) and (4), and assuming that $k_z d \ll 1$, we obtain

$$T(k_x)=\left[1-\frac{i}{2}\left(\epsilon_x\sqrt{\frac{k_0^2-k_x^2}{k_0^2}}+\sqrt{\frac{k_0^2}{k_0^2-k_x^2}}\right)k_0 d\right]^{-1}, \tag{11}$$

$$\Gamma(k_x)=\frac{\frac{i}{2}\left(\sqrt{\frac{k_0^2}{k_0^2-k_x^2}}-\epsilon_x\sqrt{\frac{k_0^2-k_x^2}{k_0^2}}\right)k_0 d}{1-\frac{i}{2}\left(\epsilon_x\sqrt{\frac{k_0^2-k_x^2}{k_0^2}}+\sqrt{\frac{k_0^2}{k_0^2-k_x^2}}\right)k_0 d}. \tag{12}$$

If we further require that $\epsilon_x\sqrt{\frac{k_0^2-k_x^2}{k_0^2}} \gg \sqrt{\frac{k_0^2}{k_0^2-k_x^2}}$ or $\epsilon_x \gg \frac{k_0^2}{k_0^2-k_x^2}$, Eqs. (11) and (12) become

$$T(k_x)=\frac{1}{1-\frac{i}{2}\epsilon_x\sqrt{k_0^2-k_x^2}d}, \quad \Gamma(k_x)=\frac{-\frac{i}{2}\epsilon_x\sqrt{k_0^2-k_x^2}d}{1-\frac{i}{2}\epsilon_x\sqrt{k_0^2-k_x^2}d}. \tag{13}$$

For a shunt impedance Z in a transmission line of characteristic impedance Z_0, the current transmission and reflection coefficients are

$$T_I=\frac{1}{1+\frac{Z_0}{2Z}}, \quad \Gamma_I=\frac{\frac{Z_0}{2Z}}{1+\frac{Z_0}{2Z}}. \tag{14}$$

Comparing Eqs. (13) and (14), the shunt Z acts like a shunt capacitor with

$$C=\epsilon_0\epsilon_x d, \tag{15}$$

as in Fig. 1(c). The condition $\epsilon_x \gg k_0^2/(k_0^2-k_x^2)$, however, cannot be satisfied throughout the entire spatial frequency region, and cannot be met at $k_x=k_0$. For k_x far from cutoff in free space (where $k_x=k_0$), for example, deep in the evanescent spectrum, enforcing $\epsilon_x \gg 1$ can lead to $\epsilon_x \gg k_0^2/(k_0^2-k_x^2)$.

Consider now that $k_z d \ll 1$, $\epsilon_z=1$, and $\epsilon_x \gg 1$ in Eqs. (3) and (4). In this case,

$$T(k_x)=\frac{1}{1-\frac{i}{2}(\epsilon_x+1)\sqrt{k_0^2-k_x^2}d}, \tag{16}$$

$$\Gamma(k_x)=\frac{\frac{i}{2}(1-\epsilon_x)\sqrt{k_0^2-k_x^2}d}{1-\frac{i}{2}(\epsilon_x+1)\sqrt{k_0^2-k_x^2}d},$$

which further simplify to

$$T(k_x)=\frac{1}{1-\frac{i}{2}\epsilon_x\sqrt{k_0^2-k_x^2}d}, \quad \Gamma(k_x)=\frac{-\frac{i}{2}\epsilon_x\sqrt{k_0^2-k_x^2}d}{1-\frac{i}{2}\epsilon_x\sqrt{k_0^2-k_x^2}d}, \tag{17}$$

if $\epsilon_x \gg 1$. Interestingly, an effective shunt capacitor with $C=\epsilon_0\epsilon_x d$ is again obtained.

If $\epsilon_x \ll -1$ and $\epsilon_z \to \infty$ or $\epsilon_z=1$, we again obtain a shunt capacitor with $C=\epsilon_0\epsilon_x d$. However, the capacitance is negative, giving a frequency-dependent shunt inductor $L=-(\omega^2\epsilon_0\epsilon_x d)^{-1}$ [see Fig. 1(c)].

III. REALIZATIONS THROUGH METAMATERIALS

In Fig. 2, we investigate the Ag/MgO metal-insulator stack as a possible realization of $\{\epsilon_x \to 0, \epsilon_z \to \infty\}$ for series inductors, $\{\epsilon_x \gg 1, \epsilon_z \to \infty\}$ for shunt capacitors, and $\{|\epsilon_x| \gg 1, \epsilon_x < 0, \epsilon_z \to \infty\}$ for shunt inductors. The real part of the di-

electric tensor components $\epsilon_{\parallel}$ and $\epsilon_{\perp}$, parallel and perpendicular to the layers, respectively, are shown in Fig. 2. The homogenized dielectric constants were determined from $\epsilon_{\parallel} = D\epsilon_{\mathrm{Ag}} + (1-D)\epsilon_{\mathrm{MgO}}$, $\epsilon_{\perp} = [D/\epsilon_{\mathrm{Ag}} + (1-D)/\epsilon_{\mathrm{MgO}}]^{-1}$, where D is the volume fraction occupied by Ag.[10] Figure 2 shows two well-defined frequency intervals: the "inductor region" and the "capacitor region." In the inductor region, tuning $\epsilon'_{\parallel}$ close to zero and with relatively large $|\epsilon'_{\perp}|$ leads to a series inductor, whereas setting $\epsilon'_{\parallel}$ much more negative than -1 and with very large $|\epsilon'_{\perp}|$ results in a shunt inductor. In the capacitor region, $\epsilon'_{\perp}$ is much greater than unity and $|\epsilon'_{\parallel}|$ is very large. In other words, the desired anisotropy for series/shunt inductor, and shunt capacitors can be achieved, respectively, by choosing $\epsilon_x = \epsilon_{\parallel}$, $\epsilon_z = \epsilon_{\perp}$ in the inductor region, and $\epsilon_x = \epsilon_{\perp}$, $\epsilon_z = \epsilon_{\parallel}$ in the capacitor region. Because the inductor effectively operates in the shorter wavelength region (from UV to visible) while the capacitor region corresponds to longer wavelength region (e.g., near the infrared band for the Ag/MgO stack), we choose the operating wavelength around the midpoint between the inductor and capacitor regions in order to implement both inductors and capacitors at the same wavelength.

To evaluate the applicability of the series/shunt inductor and shunt capacitor element concepts, Figs. 3–5 show plane-wave transmission spectra for three homogeneous slab parameter sets, in comparison with the results from a transmission line model with a lumped series inductor given by Eq. (10) with $\epsilon_z \to \infty$, a capacitor defined by Eq. (15), and a shunt inductor resulting from a shunt capacitor having negative capacitance, all embedded in a line with impedance Z_0 (the characteristic impedance of free space). For the series inductor shown in Fig. 3, the anisotropic film with smaller ϵ_x and more negative ϵ_z more closely matches the lumped element result over all k_x/k_0. The Ag/MgO stack, in the effective-medium limit at a wavelength of 785 nm, matches reasonably well, particularly for the propagating spectrum. This result can be improved by using a shorter wavelength or a smaller d. From Fig. 4, the shunt capacitor model with $\epsilon_z \to \infty$ is somewhat better than that with $\epsilon_z = 1$. The Ag/MgO stack operating at a longer wavelength could enhance the characteristics of the lumped capacitor. Figure 5 displays transmission spectra of shunt inductors associated with different parametric implementations. Notice that in Fig. 5 the transmission spectra for the homogenized slabs agree with the results calculated from lumped circuit theory in the propagating region. The discrepancy, however, is prominent for the evanescent components, especially the combination $\epsilon_x = -22$ and $\epsilon_z = 1$, which stems from the fact that the relation $k_z d \ll 1$ for exhibiting a lumped circuit response no longer holds.

We treat the metal-insulator stack as an effective medium. A solution of the exact physical problem, without recourse to homogenization, will give a more accurate prediction of the circuit model performance. However, where homogenization can be accurately applied, the plane-wave spectra we present are an adequate reference.

Practical realizations have many other material options, for example, plasmonic/polaritonic materials and semiconductors, depending on the operating frequency.[11,13,18] Determining proper operating frequency regions for designing various lumped circuit models would follow the argument we have presented.

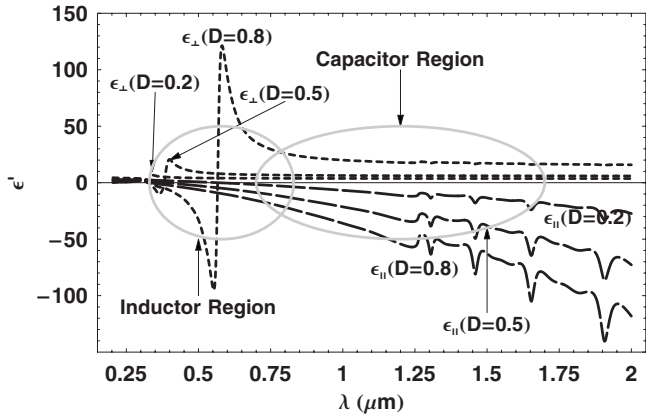

FIG. 2. The real part of the calculated homogenized dielectric constants $\epsilon_{\parallel}$ and $\epsilon_{\perp}$, parallel and perpendicular to the surface of the effective slab, for a Ag/MgO stack with Ag volume fraction D, using published data (Ref. 23).

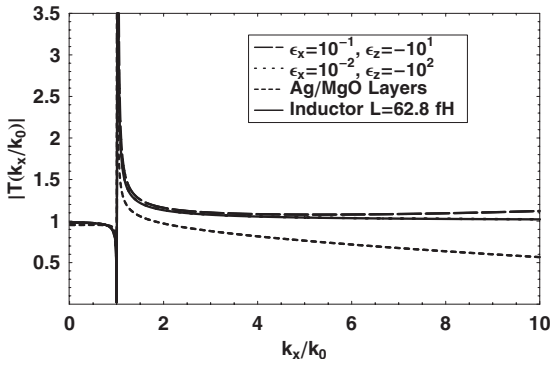

FIG. 3. Magnitude of the transmission coefficient for the exact plane-wave solution, the circuit element, and a Ag/MgO realization of a series inductor. The parameters are $d=50$ nm, $\lambda=784.7$ nm, $D=0.1$, $\epsilon_{\mathrm{Ag}} = -26.7 + i1.47$, and $\epsilon_{\mathrm{MgO}} = 2.99$ (Ref. 23), giving $\epsilon_x = \epsilon_{\parallel} = 1.94 \times 10^{-2} + i1.47 \times 10^{-1}$, $\epsilon_z = \epsilon_{\perp} = 3.36 + i2.32 \times 10^{-3}$.

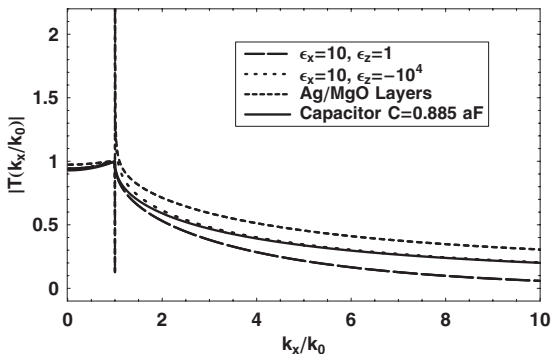

FIG. 4. Magnitude of the transmission coefficient for the exact plane-wave solution, the circuit element, and a Ag/MgO realization of a shunt capacitor. The parameters are $d=10$ nm, $\lambda=784.7$ nm, $\epsilon_{\mathrm{Ag}} = -26.7 + i1.47$, $\epsilon_{\mathrm{MgO}} = 2.99$ (Ref. 23), and $D=0.5$, giving $\epsilon_x = \epsilon_{\perp} = 6.72 + i4.65 \times 10^{-2}$, $\epsilon_z = \epsilon_{\parallel} = -11.85 + i7.35 \times 10^{-1}$.

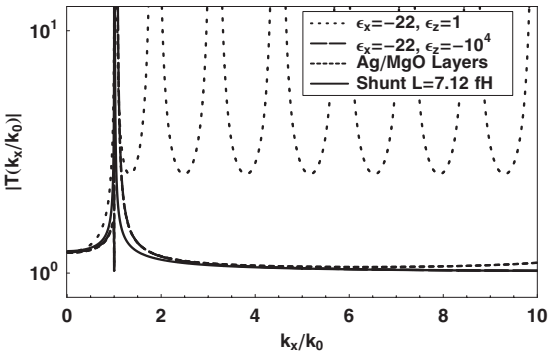

FIG. 5. Magnitude of the transmission coefficient for the exact plane-wave solution, the circuit element, and a Ag/MgO realization of a shunt inductor. The parameters are $d=125$ nm, $\lambda=784.7$ nm, $\epsilon_{Ag}=-26.7+i1.47$, $\epsilon_{MgO}=2.99$, and $D=0.85$, giving $\epsilon_x=\epsilon_{\parallel}=-22.23+i1.25$, $\epsilon_z=\epsilon_{\perp}=53.66+i5.09$.

IV. BUILDING OPTICAL CIRCUITS AND COMPONENTS

We have presented four optical circuit elements: a transmission line, a series inductor, a shunt capacitor, and a shunt inductor. Their equivalent circuit values were derived by calculating the scattering coefficients for an anisotropic slab illuminated by a TM-polarized wave. The slab is assumed infinitely wide. In an implementation, a large aspect ratio (width to length) or large local curvature (relative to the wavelength) is needed. The series inductor and the shunt capacitor slabs can be viewed as short sections of transmission line with large or small characteristic impedances, respectively.[17] The circuit parameters of the series inductors and shunt capacitors are independent of the operating frequency (unless the slab materials are dispersive) and angle of incidence, and they are uniquely determined by the dimensions and material parameters of the slab. In the case of the shunt inductor, achieved through a negative capacitance, the element value is of course frequency dependent [see Fig. 1(c)]. These circuit elements can therefore be used as a means to design structures that will effectively operate over a wide range of frequencies and incidence angles. We illustrate two possibilities: a filter and an antireflection coating that reduces the scattering cross section.

An optical low-pass filter structure is depicted in Fig. 6(a). We used both Chebyshev (equal ripple) and Butterworth (maximally flat) polynomials to determine the *L-C* values having a normalized cutoff frequency $f/f_0=1$.[17] We assumed $\epsilon_z\to\infty$, and $\epsilon_x=50$ for the capacitor sections and $\epsilon_x=10^{-3}$ for the inductor sections. For electrically thin layers, $k_z d_i \ll 2\pi$. In the case of the inductive sections, with $\epsilon_x\to 0$, this can be achieved even for geometrically thick layers, relative to the free space wavelength. The structure was designed for normal incidence with a TM plane wave. Figure 6(b) shows the magnitude of the transfer function for H_y for both normal ($k_x=0$) and oblique ($k_x=0.8k_0$) incidences. The frequency roll-off for $f/f_0>1$ is dictated by the number of sections. Figure 6(c) shows the isotropic layer solution, which exhibits identical transmission characteristics at normal incidence but deteriorates rapidly as the angle of incidence is moved off normal, illustrating the robustness to the incident angle of transmission property for anisotropic low-pass filters compared to the isotropic case. A shunt parallel *L-C* combination satisfying $Z^{-1}_{\text{Shunt}C}+Z^{-1}_{\text{Shunt}L}=0$ [see Fig. 1(c)], or $\epsilon_{x\text{Shunt}C}+\epsilon_{x\text{Shunt}L}=0$, would produce an all-pass filter in the sense of both temporal and spatial frequencies.

We note that optical filters can also be achieved with plasmonic nanoparticles,[19,20] where localized surface-plasmon interactions between individual nanoparticles and the surrounding medium are exploited. The filtering effects we de-

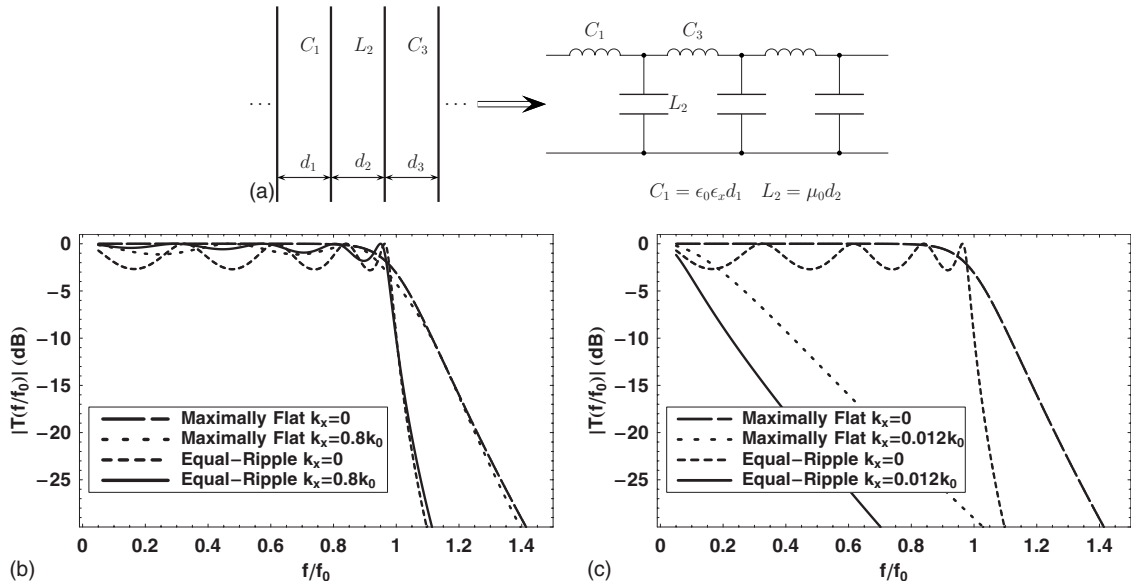

FIG. 6. (a) Synthesis of a low-pass filter *L-C* ladder network. (b) Frequency response of nine-section Chebyshev [equal-ripple, with film thicknesses l_i ($i=1,\ldots,9$)=$\{28.1,308.3,37.2,322.6,37.6,322.6,37.2,308.3,28.1\}$ (nm)] and ten-section Butterworth [maximally flat, with thicknesses l_i ($i=1,\ldots,10$)=$\{2.5,360.8,11.2,708.0,15.7,784.9,14.2,561.9,7.2,124.3\}$ (nm)] low-pass filters with normal and oblique incidences. Each anisotropic film assumes $\epsilon_z\to\infty$, and $\epsilon_x=50$ for the capacitor and $\epsilon_x=10^{-3}$ for the inductor. The wavelength corresponding to f_0 is $\lambda_0=2500$ nm. (c) Filters with the parameters in (d) and isotropic dielectric constants: $\epsilon=50$ for *C* and $\epsilon=10^{-3}$ for *L*.

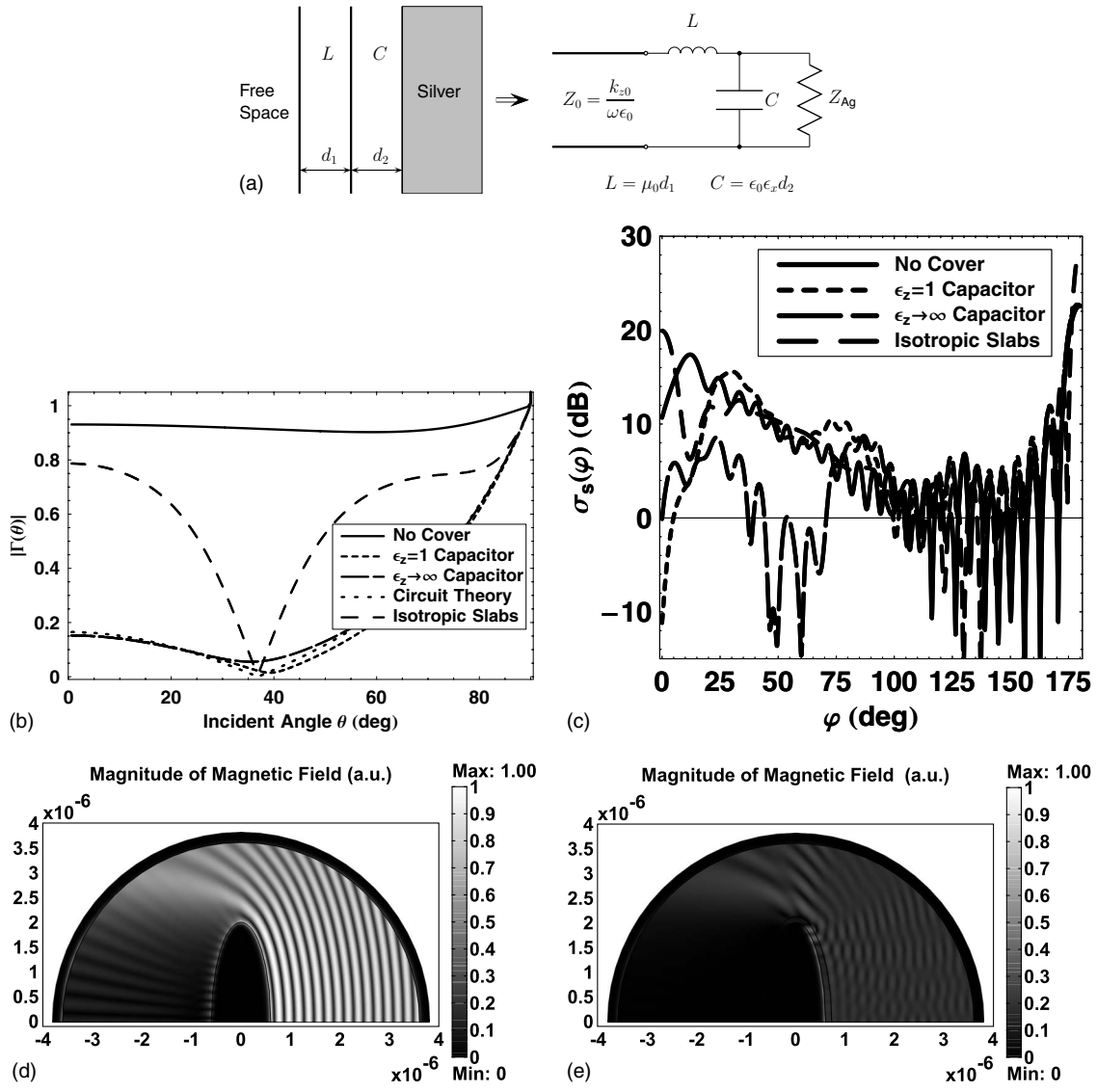

FIG. 7. (a) An L-C bilayer antireflection coating on Ag. (b) Bilayer TM reflection coefficient. Parameters: $\lambda=400$ nm, $\epsilon_{\mathrm{Ag}}=-3.77+i0.6747$ (Ref. 23), $\epsilon_z=10^3$, $\epsilon_x=50.0$ for C, $\epsilon_x=10^{-3}$ for L, $d_1=124$ nm, $d_2=3.0$ nm. The result for an isotropic quarter-wave transformer ($\epsilon=3.0$ and length 92.6 nm) on a spacer layer ($\epsilon=45.4$ and length 14.9 nm) provides a reference. (c) Simulated back-scattering cross section of the scatter with and without the bilayer cover. $|H_y(x,z)|$ for a Ag elliptical cylinder for TM wave excitation (d) without and (e) with the bilayer cover.

scribe here originate from homogenized metamaterial properties.

Impedance matching/transforming structures provide a means to substantially reduce the scattering cross section. Figure 7(a) illustrates a bilayer L-C section that can eliminate reflections from a semi-infinite Ag layer. Figure 7(b) shows the TM (H_y) reflection coefficient magnitude as a function of incidence angle (k_x/k_0) for bilayer matching to Ag. The matching was designed for $k_x/k_0=0.6$ (corresponding to the incident angle $\theta=36.8°$). The two types of capacitors ($\epsilon_z\to\infty$ and $\epsilon_z=1$) are shown, and the performance with $\epsilon_z=1$ is slightly better. The L-C slab model performance is limited by the low-impedance C section, and it approaches the ideal circuit model performance as the impedance is reduced. The practical difficulty of reducing the impedance of the C section is that its thickness becomes small, perhaps complicating fabrication. For comparison, Fig. 7(b) shows an isotropic antireflection coating, which has much greater sensitivity to angle of incidence. Achieving a low reflection for a wide range of incidence angles because of the anisotropy of the coating allows substantially reduced object visibility. To illustrate this, Fig. 7(c) shows the bistatic back-scattering cross section for a two-dimensional Ag elliptical cylinder, with an incident TM wave from the positive semiminor axis. Figures 7(d) and 7(e) show $|H_y|$ without and with the L-C coating (the wave is incident from the right). The result for a bilayer having $\epsilon_z\to\infty$ appears superior. By reducing the C-section impedance, the reflected field in Fig. 7(e) can be reduced even further. By increasing the number of L-C sections, and through appropriate design, the bandwidth properties can be controlled. The improved antireflection properties of the coating, other than potentially being applied for

stealth, could also find applications in efficient solar energy collectors.[21]

V. CONCLUSION

Anisotropic films provide a means to achieve optical circuit elements that are angle and frequency independent. This observation opens up a variety of circuit synthesis methods for implementing optical devices with important properties. We showed filter and antireflection coating examples that are robust to variation in the angle of incidence. The layers can be built with a metal-insulator stack, and our calculations with plausible geometries suggest this is possible using current fabrication technology. The circuits hold for TM polarization. Duality would lead to equivalent series capacitors and shunt inductors for TE polarization, if a suitable anisotropic permeability could be achieved (e.g., ferromagnetic materials[22]).

ACKNOWLEDGMENTS

This work was supported by the National Science Foundation (Contract No. ECS-0524442), the Department of Energy (Contract No. DE-FG52-06NA27505), and the Army Research Office (Contract No. W911NF-07-1-0019).

*webb@purdue.edu

[1] D. R. Smith, J. B. Pendry, and M. C. K. Wiltshire, Science **305**, 788 (2004).
[2] C. M. Soukoulis, M. Kafesaki, and E. N. Economou, Adv. Mater. (Weinheim, Ger.) **18**, 1941 (2006).
[3] V. M. Shalaev, Nat. Photonics **1**, 41 (2007).
[4] J. B. Pendry, Phys. Rev. Lett. **85**, 3966 (2000).
[5] A. Grbic and G. V. Eleftheriades, Phys. Rev. Lett. **92**, 117403 (2004).
[6] M. Yang and K. J. Webb, Opt. Lett. **30**, 2382 (2005).
[7] J. B. Pendry, D. Schurig, and D. R. Smith, Science **312**, 1780 (2006).
[8] E. Shamonina, V. Kalinin, K. Ringhofer, and L. Solymar, Electron. Lett. **37**, 1243 (2001).
[9] S. A. Ramakrishna, J. B. Pendry, M. C. K. Wiltshire, and W. J. Stewart, J. Mod. Opt. **50**, 1419 (2003).
[10] K. J. Webb and M. Yang, Opt. Lett. **31**, 2130 (2006).
[11] L. V. Alekseyev and E. Narimanov, Opt. Express **14**, 11184 (2006).
[12] P. A. Belov and Y. Hao, Phys. Rev. B **73**, 113110 (2006).
[13] R. Wangberg, J. Elser, E. E. Narimanov, and V. A. Podolskiy, J. Opt. Soc. Am. B **23**, 498 (2006).
[14] N. Engheta, A. Salandrino, and A. Alù, Phys. Rev. Lett. **95**, 095504 (2005).
[15] N. Engheta, Science **317**, 1698 (2007).
[16] P. A. Belov, C. R. Simovski, and P. Ikonen, Phys. Rev. B **71**, 193105 (2005).
[17] D. M. Pozar, *Microwave Engineering*, 3rd ed. (Wiley, New York, 2005), pp. 412–416.
[18] A. J. Hoffman, L. Alekseyev, S. S. Howard, K. J. Franz, D. Wasserman, V. A. Podolskiy, E. E. Narimanov, D. L. Sivco, and C. Gmachl, Nature Mater. **6**, 946 (2007).
[19] R. W. Rendell and D. J. Scalapino, Phys. Rev. B **24**, 3276 (1981).
[20] A. Alù, M. E. Young, and N. Engheta, Phys. Rev. B **77**, 144107 (2008).
[21] Y.-F. Huang *et al.*, Nat. Nanotechnol. **2**, 770 (2007).
[22] R. H. Tarkhanyan and D. G. Niarchos, Opt. Express **14**, 5433 (2006).
[23] *Handbook of Optical Constants of Solids*, edited by E. D. Palik (Academic, New York, 1998).